Compressed Sensing for Fast Electron Microscopy_{SAND2013-8293C}

Hyrum S. Anderson, Jason W. Wheeler, Kurt W. Larson

Sandia National Laboratories, P.O. Box 5800; Albuquerque, NM 87185

Abstract

Scanning electron microscopes (SEMs) are used in neuroscience and materials science to image centimeters of sample area at nanometer scales. Since imaging rates are in large part SNR-limited, imaging time is proportional to the number of measurements taken of each sample; in a traditional SEM, large collections can lead to weeks of around-the-clock imaging time. We previously reported on a single-beam sparse sampling approach that we have demonstrated on an operational SEM for collecting "smooth" images. In this paper, we analyze how measurements from a hypothetical multi-beam system would compare to the single-beam approach in a compressed sensing framework. To that end, multi-beam measurement patterns are synthesized on a single-beam SEM, and fidelity of reconstructed images are compared to the previously demonstrated approach. Since taking fewer measurements comes at the cost of reduced SNR, image fidelity as a function of undersampling ratio is reported.

INTRODUCTION

Electron microscopes are used in neuroscience, microbiology and materials science for high-resolution imaging and subsequent structural or compositional analysis. In particular, many applications that utilize a scanning electron microscope (SEM) require imaging millimeters or even centimeters of material at nanometer resolutions, leading inevitably to semi-autonomous operation of a SEM, months of around-the-clock collection time [1, 2], and vast quantities of data.

Several recent efforts have addressed the problem of collecting large mosaics of a specimen [3, 4, 5]. Engineering advances (for example, [6]) have allowed greater throughput by allowing very wide field-of-view images to reduce image tile overlap and stage movement, and by providing high scan rates. Nevertheless, even these well-engineered systems are still physically constrained—due to the single-detector arrangement, the electron probe visits each pixel location in raster-scan order and dwells for a time proportional to the desired SNR. Thus, high-SNR, nm-resolution images taken over large mosaics can lead to prohibitively long data collection times.

In this paper, we explore the use of compressed sensing as a means to the increase imaging throughput of an electron microscope. Previously, we reported an undersampling scheme that, in conjunction with compressed sensing recovery, is capable of reconstructing smooth images from few measurements at randomly distributed electron probe locations on the sample. Results from an operational SEM were first reported in [7], and relevant details are reviewed here. The chief contribution of this paper is a preliminary analysis of patterned measurements for compressed sensing in an electron microscope. In

particular, we synthesize multi-beam patterns using a traditional SEM, and compare how patterned measurements might perform versus the previously demonstrated single-beam approach.

Binev et al. investigated the applicability of compressed sensing to scanning transmission electron microscopes (STEMs) to reduce electron dose rates that might otherwise structurally alter or destroy the sample being observed [8]. We note that the dose rate motivation is equally applicable to the SEM case, in which certain biological or dielectric materials may exhibit charging artifacts if the dose rate is too high. In [8], concepts are validated via numerical simulations of a STEM.

Throughout the paper, boldface capital letters such as $\mathbf{F}$ and $\mathbf{U}$ denote matrices, lowercase boldface letters such as $\mathbf{x}$ and $\mathbf{y}$ denote vectors, while non-boldface lower-case and upper case letters, such as M and δ, denote scalars.

BACKGROUND

In this section, we provide a brief background on electron microscopy, compressed sensing, and a previously-demonstrated sparse imaging method, in which we retrofitted an existing SEM to measure the sample at randomly-selected sample locations [7].

Scanning electron microscopy

SEMs are single-detector instruments that acquire images by raster scanning a focused beam of electrons across the sample, typically in raster-order. At each location, electrons in the incident beam interact with sample, producing various signals about the composition or topography of the sample's surface. These signals may be detected and digitally assigned to the image pixel value at the corresponding sample location. The electron probe is then repositioned via electromagnetic or electrostatic deflection to the subsequent pixel location. Typically, the electron probe interaction area on the sample is much smaller than the distance between pixel locations. Two phenomena that are routinely measured by SEMs include backscatter electron (BSE) emissions, which are a result of elastic scattering of incident electrons, and secondary electrons (SE), which are lower-energy electrons that are dislodged from orbitals of specimen atoms through inelastic scattering. BSE images provide sharp contrast at transitions between the atomic number of materials, whereas, since interactions occur within only the first few nanometers of a sample's surface, SE images are primarily topographical in nature.

Noise for both BSE and SE images is multiplicative (Poisson-like), wherein the noise power is proportional to the signal intensity. In order to produce high-quality SEM images, long integration times per pixel—on the order of microseconds—are required to reduce noise. In the best case with independent measurements, one might expect SNR improvement that grows like $\sqrt{n}$; however, non-trivial detector response times and other factors necessitate longer integration times. In sum, well-engineered systems are SNR-limited in their data acquisition speed, and can require months to collect millimeters or centimeters of data for some applications.
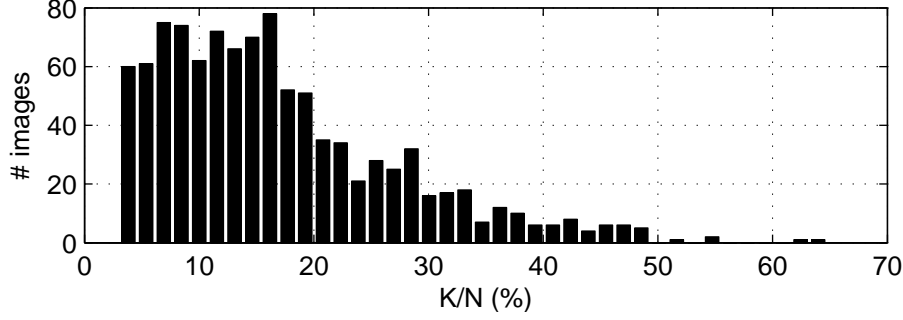
Figure 1: Histogram of compression ratios for 1022 electron microscopy images SEM, TEM and E-SEM) from the Dartmouth public domain gallery at `http://www.dartmouth.edu/~emlab/gallery`. Compression ratio is measured by counting the number of block-DCT coefficients K that account for at least 99.75% of the energy in an N-pixel image. The average compressibility is 17%, with half of all images less than 15% compressible, and three-quarters less than 20% compressible.

Compressed sensing

When expressed in an appropriate basis, the number of significant coefficients in an electron microscope image is much smaller than the number of image pixels (see Fig. 1).

The number of significant coefficients of an electron microscopy image, as expressed in some compression basis, is typically much smaller than the number of image pixels. Foundational contributions in compressed sensing guarantee that an N-pixel image $\mathbf{x}$—which can be described by K coefficients in some compression basis $\mathbf{\Psi}$ as $\mathbf{x} = \mathbf{\Psi}\alpha$—can be recovered in only $M = O(K \log \frac{N}{K})$ linear measurements of the form $\mathbf{y} = \mathbf{\Phi x} = \mathbf{\Phi \Psi}\alpha$. The tightest guarantee to date on recovering the coefficient vector α from $\mathbf{y}$ holds for basis pursuit reconstruction when $\mathbf{A} = \mathbf{\Phi \Psi}$ satisfies the restricted isometry property (see [9]). In particular, solve

$$\min_{\alpha} \quad \|\alpha\|_1 \quad \text{s.t.} \quad \mathbf{A}\alpha = \mathbf{y}. \tag{1}$$

It should be noted that for arbitrary $\mathbf{A}$, certifying that the restricted isometry property holds is combinatoric in M. Although mutual coherence $\mu(\mathbf{\Phi}, \mathbf{\Psi})$ provides a looser guarantee on reconstruction from $M = O(\mu K \log N)$ measurements, it is trivial to compute [10]. Traditionally in compressed sensing, $\mathbf{\Phi}$ is designed randomly as a sub-Gaussian matrix, such as Gaussian or Bernoulli (uniform ± 1), so that the restricted isometry property or minimal mutual coherence is satisfied with high probability for any compression basis $\mathbf{\Psi}$, providing favorable conditions for guaranteed recovery.

Single-beam sparse imaging

In our previously demonstrated embodiment [7], we use a single electron probe positioned at random locations within the field-of-view, so that in theory, $\mathbf{\Phi}$ consists of M randomly drawn rows of the identity matrix; $\mathbf{\Phi}$ is chosen as a block-DCT basis, which provides good compressibility of smooth electron micrographs, and also results in low mutual

coherence for compressed sensing inversion. Motivated by good JPEG compressibility of SEM images, and by the low mutual coherence between the DCT basis and image-domain sampling, we choose $\boldsymbol{\Psi}$ to be a block-DCT basis with 32×32 pixel blocks.

In [7], we proposed a sparse imaging retrofit to an existing SEM, in which the electron probe visits a fraction M/N of randomly-selected sample locations. In experiments, the incident beam was deflected onto the sample using the standard scanning coils and current amplifiers in the column, which we interfaced with a custom digital-to-analog converter (DAC). The SEM detector signal was sampled using an analog-to-digital converter (ADC) that was synchronized to the DAC. Variable dwell time was achieved by digitally averaging multiple samples at the same pixel location: a basic dwell time of 400 ns using one sample per pixel results in low-SNR images, while a high-SNR dwell time of 6.4 μs achieved by averaging 16 samples per pixel.

Reconstructing electron micrographs from measurements $\mathbf{y} = \boldsymbol{\Phi}\mathbf{x} + \mathbf{n}$, where $\mathbf{n}$ has noise with power σ^2, was achieved by solving a total-variation regularized version of basis pursuit

$$\min_{\mathbf{x}} \quad \|\boldsymbol{\Psi}^T \mathbf{x}\|_1 + \|\nabla \mathbf{x}\|_1$$
$$\text{s.t.} \quad \|\mathbf{y} - \boldsymbol{\Phi}\mathbf{x}\| \leq \sigma^2.$$

The total variation regularizer $\|\nabla \mathbf{x}\|_1 = \sum_i \sqrt{|(\nabla_h \mathbf{x})_i|^2 + |(\nabla_v \mathbf{x})_i|^2}$ was included for denoising and to promote smooth boundaries between blocks. In [7], we derived a split Bregman reconstruction method for efficient image recovery. Sufficiently high-quality reconstructions were achieved with 20–50 iterations of our algorithm.

Nontrivial dynamics of the electron probe scanning system created a mismatch between the desired and actual measurement locations on the sample. We found the dynamics of the beam to be slow slow compared to the sampling period, and compensated by fitting a fifth-order linear model to calibration data, and using the model to predict the actual probe location:

$$\frac{d^5 x(t)}{dt^5} = a_0(\hat{x}(t) - x(t)) - a_1 \frac{dx(t)}{dt} - a_2 \frac{d^2 x(t)}{dt^2} - a_3 \frac{d^3 x(t)}{dt^3} - a_4 \frac{d^4 x(t)}{dt^4},$$

where $x(t)$ is the true one-dimensional probe position (in pixels) at time t, $\hat{x}(t)$ is the desired position, and the parameters $\{a_0, \ldots, a_4\}$ were fitted via calibration data. The same dynamical model was used for both horizontal and vertical beam deflection.

Results for the sparse sampling collection and reconstruction are shown in Figure 2. For $M/N = 10\%$, the reconstruction exhibits some smearing along the vertical path of the electron probe, which can be attributed to large electron probe velocities and small errors in the 5th order model. Acceptable image reconstruction is achieved for $M/N \geq 30\%$, corresponding to over $3\times$ increase in data throughput. Notice also that the for smaller M/N, the lower average electron dose rates contribute to less charging on the sample (manifest by the slight glow on the left-hand side of the original image).

The speedup achieved by sparsely undersampling the sample was proportional to N/M, as expected. The measured image acquisition time for collecting every pixel of a 1000×1000 image with 16 samples per pixel was 6.9s (expected 6.4s at 2.5 MHz). Using sparse sampling factors of 10%, 30% and 50%, we measured image collection
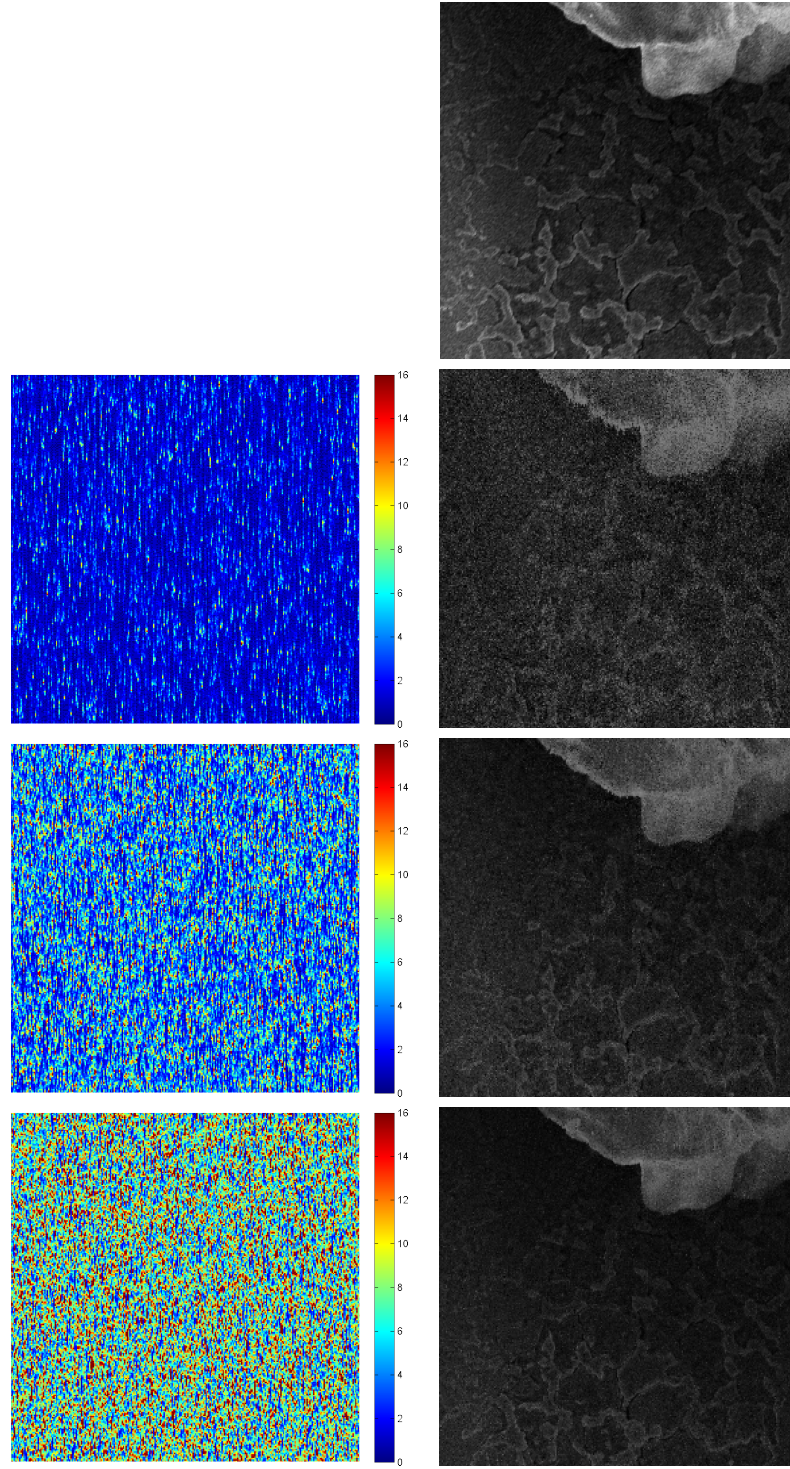
Figure 2: (top) Standard SEM image of the Gibeon sample; (2nd row) 10% sparse, modeled sample locations (left) and reconstruction (right); (3rd row) 30% sparse, modeled sample locations (left) and reconstruction (right); (4th row) 50% sparse, modeled sample locations (left) and reconstruction (right). The colors in the left column represent the number of times the probe visited the given pixel. The electron probe scans in the vertical direction. In addition to sample quality, notice the difference in sample charging.

times 0.7s (9.9× speedup), 2.1s (3.3× speedup), and 3.5s (2.0× speedup), respectively, for 1000×1000 images.

In summary, the sparse sampling approach may be conveniently implemented as a retrofit to an existing SEM. Reasonable performance can be achieved with a 2–3× speedup, but greater performance is limited by the accuracy of a beam dynamical model, and lower the SNR caused by electron beam brightness limitations on the SEM.

ANALYSIS OF MULTI-BEAM MEASUREMENT PATTERNS

In this section, we explore the effect of compressed sensing recovery in electron microscopy with a single detector when multiple electron probes (beamlets) simultaneously interact with the sample. In many compressed sensing imaging systems, the measurement matrix $\mathbf{\Phi}$ is designed randomly as a sub-Gaussian matrix, such as Bernoulli (uniform 0/1), so that the restricted isometry property or minimal mutual coherence is satisfied with high probability for any compression basis $\mathbf{\Psi}$, providing favorable conditions for guaranteed recovery. In essence, the random measurement patterns allow for recovering a broader class of images.

In this section, we analyze the performance of electron patterns for compressed sensing in an abstract electron microscope with the following idealized conditions:

- we employ a hypothetical multi-beam source with individually steerable beamlets to projects programmable electron patterns on the sample; and

- we employ a single detector with linear response and sufficient dynamic range, so that the detector response to a superposition of beamlet/sample interactions is identical to the sum of detector responses to each individual beamlet/sample interaction.

We ignore significant engineering challenges to realizing these conditions. For these simulations, we also ignore the nontrivial beam dynamics, comparing only the effects of single vs. multiple beams for compressed measurements. The abstract embodiment has parallels to the Rice single-pixel camera, in which Bernoulli (0/1) measurement patterns were multiplexed with the use of a single photodetector [11].

For experiments, we used a commercially available Zeiss GmbH (Oberkocken, Germany) column with a Schottky thermal field emission source and Gemini$^{\text{TM}}$ optics. We collected 1000 800×800-pixel images of a single area of interest on a Gibeon meteorite sample using a SE detector. To mitigate any sample drift during the image collection time, the stack of 1000 images was registered to one another to within 1/10 of a pixel. A nominal beam energy of 10 keV was used with a 10 μm aperture, resulting in a beam current of approximately 200 pA. Variable dwell time was achieved by digitally averaging multiple samples per pixel. We collected 3 separate image stacks in this manner, corresponding to dwell times of approximately 430 ns, 860 ns, and 1.7 μs.

A measurement at a given pixel location were synthesized by drawing from one of the 1000 measurements at random. A synthetic image created in this manner is shown in Figure 3. Multibeam measurements from a combination of pixels were then synthesized from image stacks in the following manner. Each measurement consists of the response of B beamlets that are incident on random locations on the sample, drawn uniformly
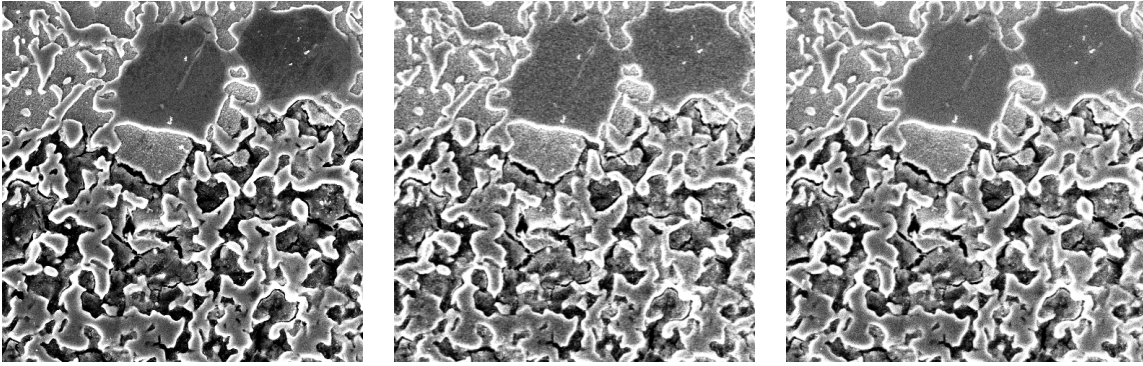
Figure 3: (left) High SNR SEM image of region of interest on the Gibeon sample; (middle) a low-SNR image from a SEM scan; (right) a synthetic image generated from multiple collacated SEM image scans.

with replacement. The detector response of the cumulative electron/sample interactions at pixel locations $p_1, \ldots, p_B$ is synthesized as $\sum_{i=1}^{B} x_{p_i}$, where x_i is a drawn uniformly from the 1000 measurements at the ith pixel.

Compressive sampling matrices $\mathbf{\Phi}$ are constructed using 1,2,4,8 and 16 beamlets for an $N = 128 \times 128$ image. The compression basis $\mathbf{\Psi}$ is chosen to be a block DCT basis with 32×32 pixel blocks, as used in our previous single-beam work. However, image are reconstructed using generic basis pursuit via the SPGL1 solver [12], rather than the split-Bregman approach specially formulated for sparse imaging with a single beamlet. Reconstructed images for $\frac{M}{N} = 50\%$ at various dwell times and number of beamlets are shown in Figure 4.

Qualitatively, there is a tradeoff between image detail and noise as more beamlets are used for compressed imaging. With a single electron probe, images are smooth and relatively noise-free, but lack some detail in finer sample features. Note that since images were reconstructed using generic basis pursuit rather than our split-Bregman approach with total-variation regularization, DCT-block boundary artifacts can be seen in the single beam images. The boundary effects diminish as multiple beams are utilized for compressed samples, since measurements using multiple beams simultaneously couple pixels across block boundaries. The low-quality reconstruction with 2 beamlets exhibit a great degree of speckle noise, which might be ameliorated with additional regularization, as in our split-Bregman approach. Results using 16 beamlets reveal the most detail, but also exhibit artificial graininess due to noise. Amplification of noise is a known problem in compressed sensing applications.

CONCLUSIONS

Previously, we have demonstrated sparse sampling in an operational SEM, with acceptable image quality achieved at $3\times$ speedup for the sample we imaged [7]. This was accomplished by commanding the electron probe to visit a randomly-selected subset of pixel locations, predicting the actual locations via a 5th-order dynamical model, then recovering the image using a split-Bregman formulation of regularized basis pursuit that
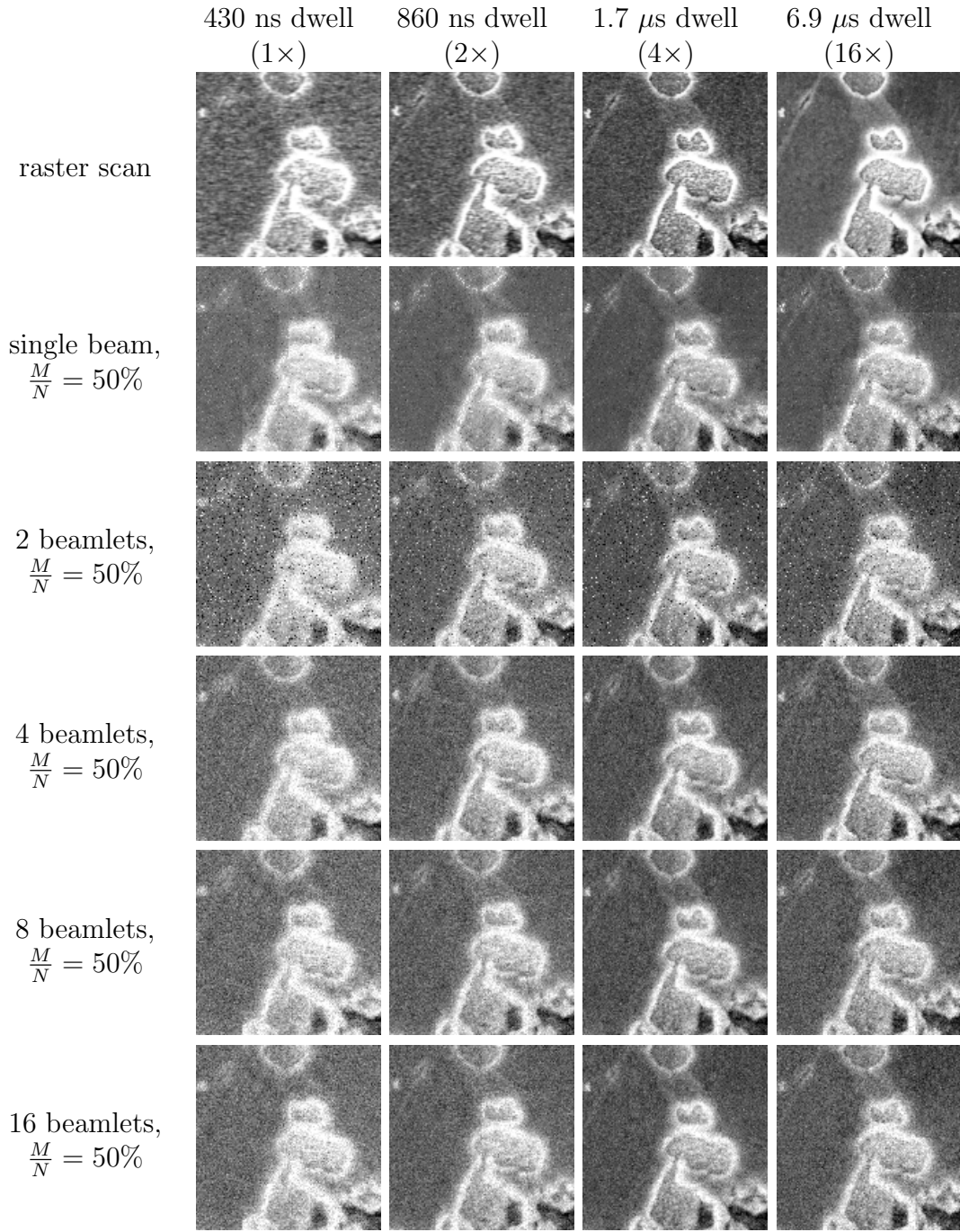
Figure 4: Compressed-sensing reconstruction results via generic basis pursuit for 1, 2, 4, 8, and 16 simultaneously-illuminating electron probes.

leveraged block-DCT as a compression basis.

In this paper, we explored the effects of illuminating the sample with multiple independently steerable beamlets in a hypothetical multibeam system. Increasing the number of beamlets has some favorable properties, such as increased detail and greater universality, but images appear grainy due to amplification of noise through compressed sensing inversion.

ACKNOWLEDGEMENTS

References

[1] K. L. Briggman and W. Denk, "Towards neural circuit reconstruction with volume electron microscopy techniques," *Current Opinion in Neurobiology* **16**, 562–570 (2006).

[2] J. R. Anderson, B. W. Jones, C. B. Watt, M. V. Shaw, J.-H. Yang, D. DeMill, J. S. Lauritzen, Y. Lin, K. D. Rapp, D. Mastronarde, P. Koshevoy, B. Grimm, T. Tasdizen, R. Whitaker, and R. E. Marc, "Exploring the retinal connectome," *Molecular Vision* **17**, 355–379 (2011).

[3] K. Ogura, M. Yamada, O. Hirahara, M. Mita, N. Erdman, and C. Nielsen, "Gingantic montages with fully automated FE-SEM," *Microsc. Mincroanal.* **16 (Suppl 2)**, 52–63 (2010).

[4] A. R. Shiveley, P. A. Shade, A. L. Pilchak, J. S. Tiley, and R. Kerns, "A novel method for acquiring large-scale automated scanning electron microscope data," *Journal of Microscopy* **244**, 181–186 (2011).

[5] K. J. Hayworth, N. Kasthuri, R. Schalek, and J. W. Lichtman, "Automating the collection of ultrathin serial sections for large volume TEM reconstructions," *Microsc. Microanal.* **12 (Suppl 2)**, 86–87 (2006).

[6] M. Wiederspahn, "Anyalytical power for the sub-nanometer world," *Imaging & Microscopy* **11**, 25–26 (2009).

[7] H. S. Anderson, J. Ilic-Helms, B. Rohrer, J. Wheeler, and K. Larson, "Sparse imaging for fast electron microscopy," in *IS&T/SPIE Electronic Imaging*, 86570C–86570C, International Society for Optics and Photonics (2013).

[8] P. Binev, W. Dahmen, R. DeVore, P. Lamby, D. Savu, and R. Sharpley, *Modeling Nanoscale Imaging in Electron Microscopy*, ch. Compressed Sensing and Electron Microscopy, 73–126. Springer (2012).

[9] E. Candés, "The restricted isometry property and its implications for compressed sensing," *Comptres rendus-Math.* **346**(9–10), 589–592 (2008).

[10] D. Donoho, M. Elad, and V. Temlyakov, "Stable recovery of sparse overcomplete representations in the presence of noise," *Information Theory, IEEE Transactions on* **52**(1), 6–18 (2006).

[11] M. F. Duarte, M. A. Davenport, D. Takhar, J. N. Laska, T. Sun, K. F. Kelly, and R. G. Baraniuk, "Single-pixel imaging via compressive sampling," *Signal Processing Magazine, IEEE* **25**(2), 83–91 (2008).

[12] E. Van Den Berg and M. Friedlander, "SPGL1: A solver for large-scale sparse reconstruction," *Online: http://www. cs. ubc. ca/labs/scl/spgl1* (2007).